Very large domain wall velocities in Pt/Co/GdOx and Pt/Co/Gd trilayers with Dzyaloshinskii-Moriya interaction

Thai Ha Pham[1,2], J. Vogel[1,2], J. Sampaio[3], M. Vaňatka[1,2], J.-C. Rojas-Sánchez[1,2], M. Bonfim[4], D. S. Chaves[1,2], F. Choueikani[5], P. Ohresser[5], E. Otero[5], A. Thiaville[3] and S. Pizzini[1,2]

[1] *CNRS, Institut Néel - 38042 Grenoble, France*
[2] *Univ. Grenoble Alpes, Institut Néel - 38042 Grenoble, France*
[3] *Laboratoire de Physique des Solides, CNRS, Univ. Paris-Sud, Université Paris-Saclay - 91405 Orsay, France*
[4] *Departamento de Engenharia Elétrica, Universidade Federal do Paraná - Curitiba, Brazil*
[5] *Synchrotron Soleil - L'Orme des Merisiers, Saint-Aubin, 91192 Gif-sur-Yvette, France*

Abstract – We carried out measurements of domain wall (DW) velocities driven by magnetic-field pulses in symmetric Pt/Co/Pt and asymmetric Pt/Co/AlOx, Pt/Co/GdOx and Pt/Co/Gd trilayers with ultrathin Co layers and perpendicular magnetic anisotropy. The maximum observed velocity is much larger in the asymmetric samples, where the interfacial Dzyaloshinskii-Moriya interaction (DMI) stabilises chiral Néel walls. In quantitative agreement with analytical models, in all samples the maximum observed DW speed scales as D/M_s, where D is the strength of the DMI and M_s the spontaneous magnetisation. In Pt/Co/Gd, where the anti-parallel coupling between the magnetic moments of Gd and Co leads to a decrease of the total magnetisation, very large DW speeds (up to $700\,\mathrm{m/s}$) are obtained.

Introduction. – Domain wall (DW) dynamics in multilayer films with perpendicular magnetic anisotropy (PMA) is an important topic today, as these micromagnetic objects may be used as carriers of binary information in future ultrahigh density storage devices [1]. In non-centrosymmetric multilayers with ultrathin magnetic films DWs can acquire Néel internal structure with a fixed chirality stabilised by the interfacial Dzyaloshinskii-Moriya interaction (DMI) [2]. This new feature strongly modifies the DW dynamics, driven both by field and by spin-polarised current. In particular, in systems with strong DMI, DWs move at large speeds when driven by current pulses [3–6].

Field-driven DW dynamics has been studied mainly in the very low-velocity regime [7–10], while few studies have explored the effect of the DMI on the high-velocity regime [11–14]. The maximum DW velocity is limited by the breakdown occurring at the so-called Walker field H_W, beyond which the DW motion is no longer stationary and its internal structure undergoes continuous precession. In symmetric ultrathin films with PMA this breakdown is reached for small fields (around 10–$20\,\mathrm{mT}$ for Pt/Co/Pt samples [15]), as the energy difference between Néel and Bloch wall configurations is small and it is thus easy to switch from one to the other. For this reason the velocities observed at high fields are relatively small [15].

This limitation is overcome in multilayer systems with strong interfacial DMI. This interaction, an antisymmetric exchange term favouring non-collinear magnetic textures [16,17], can be non-vanishing in asymmetric stacks in which an ultrathin magnetic film is deposited on a large spin-orbit metal layer [18]. The DMI acts as an effective chiral field H_{DMI} normal to the DW direction and localised on the DW, which induces chiral Néel walls that become stable against precession up to larger fields [2,6]. This allows them to reach larger velocities than in symmetric stacks without DMI. A first demonstration was given by Miron *et al.* [3] who showed that in Pt/Co/AlOx trilayers DWs move with much larger velocities than in Pt/Co/Pt. The presence of a large DMI in Pt/Co/AlOx was confirmed experimentally using chiral nucleation experiments [19] and Brillouin light scattering (BLS) spectroscopy [20].

The aim of this work is to compare DW velocities in symmetric and asymmetric stacks with PMA and to address the effect of the DMI strength on the DW velocity

at the Walker field and above. We show that velocities much larger than those measured for symmetric Pt/Co/Pt can be obtained in asymmetric Pt/Co/MOx (M=Al, Gd), and that these increase considerably in samples where Co and Gd interfacial moments couple antiparallelly. We also show that in the asymmetric samples the velocity saturates for large out-of-plane fields, in contrast with 1D micromagnetic simulations that predict a drop of the speed at the Walker field, but in agreement with 2D simulations.

Sample growth and characterisations. – Measurements were carried out on a Pt(4)/Co(1)/Pt(4) symmetric stack and three asymmetric stacks, Pt(4)/ Co(0.8)/AlOx(3), Pt(4)/Co(1)/GdOx(4)/Al(7) and Pt(4)/Co(1)/Gd(3)/Al(7) (thickness in nm). All samples were grown on Si/SiO$_2$ substrates by magnetron sputtering at room temperature and the Al and Gd layers were oxidised with an oxygen plasma. Note that the Co thicknesses are larger than the 0.6 nm value of previous works [4,14], so as to bring the Walker breakdown into the observable field region. The magnetic properties of the samples were measured with VSM-SQUID at variable temperature and X-ray magnetic circular dichroism (XMCD) at the Co $L_{2,3}$ and Gd $M_{4,5}$ absorption edges. The XMCD measurements were carried out at the DEIMOS beamline of the SOLEIL synchrotron (Saint Aubin, France).

The DW velocities were measured on continuous films, using magneto-optical Kerr microscopy. The film magnetisation was first saturated in the out-of-plane direction. An opposite magnetic-field pulse was then applied to nucleate one or several reverse domains. The DW velocity was deduced from the expansion of the initial bubble domain, after the application of further magnetic-field pulses. Using a 200 μm diameter coil and a fast current source, out-of-plane magnetic-field pulses of strength up to $B_z = 300$ mT and duration down to 20 ns were applied. In order to visualise the various regimes of DW propagation predicted by the theoretical models, DW speeds were measured as a function of B_z. In order to address the DMI strength in the various samples, the DW speeds driven by the B_z pulses were measured in the presence of a static in-plane field B_x normal to the DW plane [7–10].

Domain wall dynamics in symmetric and asymmetric trilayers with PMA. – Figure 1(a), (b) show the differential Kerr images corresponding to the expansion of a domain in Pt/Co/Pt (a) and Pt/Co/AlOx (b) after the application of a B_z pulse, respectively without in-plane field (left images) and in the presence of an in-plane field (right images). In figs. 1(c), (d) we show the DW speed-*vs.*-B_x curves measured for the up/down and down/up DWs propagating in the $\mp x$-directions, driven by 20 ns long B_z field pulses of, respectively, 88 mT and 132 mT strength. For Pt/Co/Pt the speeds of up/down and down/up DWs are, within the error bars, the same for every value of B_x. The curves for the two DWs are symmetric with respect to the $B_x = 0$ axis.
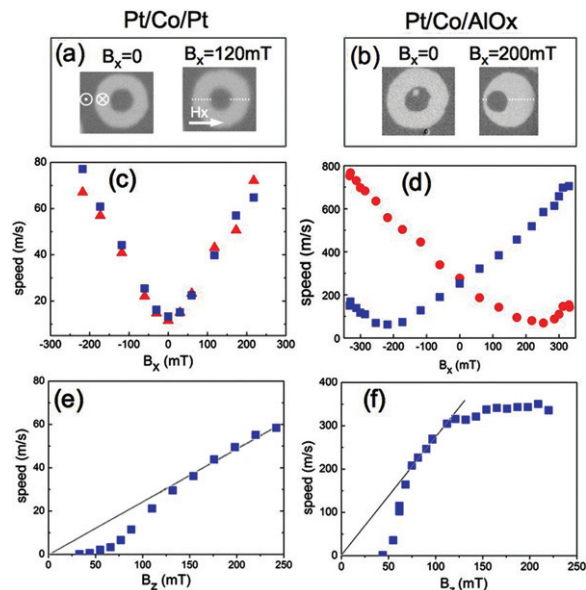

Fig. 1: (Colour online) (a), (b): differential Kerr images showing the expansion of a domain during the application of an out-of-plane field B_z, without and with the simultaneous application of an in-plane field, in Pt/Co/Pt (a) and Pt/Co/AlOx (b); (c), (d): DW velocity *vs.* in-plane field B_x for Pt/Co/Pt ($B_z = 88$ mT) (c) and Pt/Co/AlOx ($B_z = 132$ mT) (d). Blue squares: down/up DWs, red dots: up/down DWs. (e), (f): DW velocity *vs.* B_z for Pt/Co/Pt (e) and Pt/Co/AlOx ($B_x = 0$) (f). The thin lines in (e), (f) emphasise the slope of the linear regime.

In general, in symmetric magnetic layers with PMA, Bloch walls are more stable as they do not give rise to magnetostatic energy while Néel walls do. In order to decrease their Zeeman energy, the magnetisation of such walls aligns parallel to an in-plane field applied perpendicular to them, as soon as this field is larger than the DW demagnetising field. In the high-field regime, the DW velocity increases, as the DW width increases. The symmetric curves measured for Pt/Co/Pt reflect the equivalent dynamics of up/down and down/up DWs, and are in line with the presence in this sample of Bloch walls.

In Pt/Co/AlOx the DW propagation is anisotropic in the direction of B_x. The speed-*vs.*-B_x curves show a minimum for ∓ 220 mT respectively for down/up and up/down DWs, and the trend for up/down and down/up DWs is similar for H_x fields applied in opposite directions. This is the fingerprint of the presence of chiral Néel walls stabilised by the Dzyaloshinskii-Moriya interaction, that acts as a local transverse field $H_{\rm DMI}$ having opposite directions for up/down and down/up DWs. The DW velocity presents a minimum when the applied in-plane field compensates the $H_{\rm DMI}$ field, *i.e.*, for the B_x field for which the DW magnetisation reaches the Bloch orientation [7]. From the value of this field we can then deduce the average DMI energy density D, since $H_{\rm DMI} = D/(\mu_0 M_{\rm s} \Delta)$ (where D is the DMI strength, $M_{\rm s}$ the spontaneous magnetisation and $\Delta = \sqrt{A/K_0}$ the

Table 1: Co thickness t_{Co}, spontaneous magnetisation M_{s}, effective anisotropy energy K_0, exchange stiffness A (two values taken from the literature), DW parameter Δ, damping constant α, DMI field $\mu_0 H_{\mathrm{DMI}}$, DMI energy density D extracted from the DMI field, DMI energy density D^* obtained from other measurements: [a] nucleation [19], [b] BLS, on a similar sample [10], [c] BLS on the same sample. Note that the best agreement between D and D^* is obtained using $A = 16\,\mathrm{pJ/m}$.

Sample	t_{Co}	M_{s}	K_0	A	Δ	α	$\mu_0 H_{\mathrm{DMI}}$	D	D^*	$\mu_0 H_{\mathrm{W}}^{\mathrm{th}}$	$\mu_0 H_{\mathrm{W}}^{\mathrm{exp}}$
	nm	MA/m	MJ/m^3	pJ/m	nm		T	mJ/m^2	mJ/m^2	mT	mT
Pt/Co/AlOx	0.8	1.18	0.41	22	7.2	0.45	0.22	1.91		140	
				16	6.2	0.39		1.63	1.65[a]	120	120
Pt/Co/GdOx	1	1.26	0.41	22	7.2	0.33	0.20	1.73		97	
				16	6.2	0.28		1.48	1.5[b]	83	79
Pt/Co/Gd	1	0.64	0.26	22	9.2	0.34	0.30	1.78		156	
				16	7.9	0.30		1.52	1.5[c]	133	116

DW width parameter) [6]. The large DMI energy density ($D = 1.63\,\mathrm{mJ/m^2}$ for 0.8 nm Co thickness) —extracted using $\mu_0 H_{\mathrm{DMI}} = 220\,\mathrm{mT}$ and the material parameters shown in table 1— is in good agreement with the values previously obtained for similar samples [19,20]. The sign of the H_{DMI} field confirms the presence of left-handed DW chirality [14,19,21].

Let us now see what is the consequence of the different DW structure on the mobility of the DWs driven by a pure easy-axis field. Figures 1(e), (f) show the DW velocity as a function of B_z, measured for the Pt/Co/Pt and Pt/Co/AlOx trilayers. The trend for Pt/Co/Pt is very similar to that found in [15] for Pt/Co(0.8 nm)/Pt. The velocity changes exponentially with the field up to around 130 mT (creep regime); beyond this field the DW mobility is constant up to the largest applied field (250 mT). According to the measured material parameters, the Walker field in this sample ($H_{\mathrm{W}} = \alpha M_{\mathrm{s}} N_{\mathrm{NDW}}/2$, where N_{NDW} is the demagnetisation factor of a Néel wall and α the damping parameter) [15] should be of the order of 12.5 mT and is therefore hidden by the creep regime. We therefore expect that in the constant mobility region the DWs evolve in the so-called precessional flow, where the DW internal structure continuously changes between Bloch to Néel. In this regime the asymptotic mobility $m = \gamma_0 \Delta/(\alpha + 1/\alpha) = 0.25\,\mathrm{m/s/mT}$ is relatively small and in good agreement with that obtained in [15]. From a linear fit of the high-field curve we obtain $\alpha \approx 0.4$. On the other hand, fitting the data under the assumption that the linear regime is associated to the steady flow ($m = \gamma_0 \Delta/\alpha$) gives rise to an irrealistic value of the damping parameter ($\alpha = 4$).

The speed-$vs.$-B_z curve measured for Pt/Co/AlOx strongly differs from that measured for Pt/Co/Pt, with the striking result that the maximum DW velocity in the given field range is a factor 5 larger. For fields between 70 and 120 mT a clear linear regime appears, characterised by a DW mobility of 3 m/s/mT. We correlate the large velocities with the strong DMI evidenced by the previous measurements. Thiaville $et\ al.$ [2] predict that in the presence of DMI the Walker breakdown shifts to larger fields and

that, for $D \gg 0.14\mu_0 M_{\mathrm{s}}^2 t_{\mathrm{Co}}$, $H_{\mathrm{W}} \approx \alpha H_{\mathrm{D}} = \pi\alpha H_{\mathrm{DMI}}/2$ (see footnote [1]). Using $\alpha \approx 0.35$, as extracted from the DW mobility in the linear regime and the measured $\mu_0 H_{\mathrm{DMI}}$, we obtain $\mu_0 H_{\mathrm{W}} \approx 120\,\mathrm{mT}$ which is, as predicted, much larger than that of Pt/Co/Pt, and very close to the field for which the linear regime ends and the DW velocity practically saturates in our measurements. In agreement with the prediction of 1D micromagnetic models [2] the measured Walker velocity changes linearly with the in-plane field. This is shown in the inset of fig. 3(b) for the Pt/Co/Gd trilayer described below, where the velocity reaches 1100 m/s for $B_x = 300\,\mathrm{mT}$. The DMI-induced extension of the steady flow regime therefore allows explaining the large DW velocities observed for the asymmetric samples.

Saturation of DW speeds at large fields. – In contrast with the predictions of micromagnetic 1D models, in Pt/Co/AlOx, as well as in Pt/Co/Gd and Pt/Co/GdOx shown below, the DW velocity saturates for large B_z fields. We carried out large-scale 2D micromagnetic simulations using the MuMax3 code [22] with the parameters of Pt/Co/GdOx determined in this paper (see table 1). To avoid the effects of the borders and the associated DW tilting [11,14] we simulated a propagating DW in a moving $1 \times 1\,\mu\mathrm{m}^2 \times 1\,\mathrm{nm}$ box with periodic boundary conditions linking the top and bottom edges. The lateral mesh size was 2 nm. Different values of the damping α (0.15 to 0.35) were tested. In addition, perfect and disordered samples were considered (the latter realised with a spatial fluctuation of the uniaxial anisotropy value, as was done in [14]). Figure 2(a) shows the results for the perfect system. The DW speed initially increases linearly with field, up to the Walker field, which is proportional to the damping parameter. The Walker velocity is independent of damping, as expected from the 1D collective coordinates

_____

[1] The field $H_D = (\pi/2)D/(\mu_0 M_{\mathrm{s}}\Delta)$ was first defined by [2]. This competes directly with the anisotropy field of the DW moment, due to the demagnetising energy. On the other hand, when comparing the effect of the DMI to that of an external in-plane field, it was shown by [6] that the DMI is equivalent to applying a chiral field $H_{\mathrm{DMI}} = D/(\mu_0 M_{\mathrm{s}}\Delta)$. Therefore, $H_D = (\pi/2)H_{\mathrm{DMI}}$.
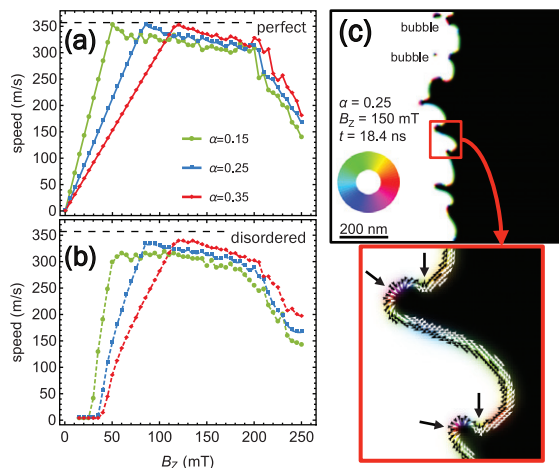
Fig. 2: (Colour online) Simulated DW dynamics in a $1\,\mu m \times 1\,\mu m$ moving window, with the parameters of Pt/Co/GdOx: $A = 16\,\text{pJ/m}$, $M_s = 1.26\,\text{MA/m}$, $D = 1.5\,\text{mJ}\cdot\text{m}^{-2}$, $K_u = 1.44\,\text{MJ}\cdot\text{m}^{-3}$. A perfect sample (a), (c) and a disordered sample (b) are considered. In the magnetisation snapshot (c), white/black corresponds to the perpendicular magnetisation component and the colours to the in-plane component (see colour wheel in the inset). Large arrows indicate the Bloch lines.

(q, Φ) model [2]. Above the Walker field, the speed reaches a plateau with $\approx 300\,\text{m/s}$, in quantitative agreement with the experimental results (fig. 3(a)). This plateau is a characteristic of the dissipation mechanisms in 2D Dzyaloshinskii DWs above the Walker field [11,12]. A representative snapshot of the DW structure above the Walker field is shown in fig. 2(c). The DW presents a complex meander shape and its magnetisation rotates several times along the wall. As discussed by Yoshimura *et al.* [11], pairs of Bloch lines (marked with large arrows in the magnified view) are continuously nucleated in the DW. These lines, with their Néel-like orientation, can have two very different widths, depending on whether they rotate in the sense favoured by DMI or not. The DW sections containing such lines are slower, hence the meandering DW shape. The lines disappear either by collapse of winding pairs with emission of spin waves (like in [11]), or by the creation of bubble domains (visible in the figure) that detach by pinching off the wall meanders, and eventually collapse. When the bubbles contain Bloch lines, these annihilate and transform the bubbles into skyrmions with structure stabilised by DMI, before the skyrmions themselves collapse. The creation of bubbles is a second dissipation mechanism that was not seen in the calculations by Yoshimura *et al.*, as the DMI considered in that work was relatively small (typically 16% of the critical value D_c for destabilisation of the uniform magnetisation), whereas here $D/D_c = 0.45$. The reduced DW energy in the case considered here favours the meandering of the DW and the subsequent creation of bubbles. Altogether, and as explained by [11] who called it a solitonic behaviour, the DW structure is on the average that of a chiral Bloch wall. Indeed, with dominant DMI, this is
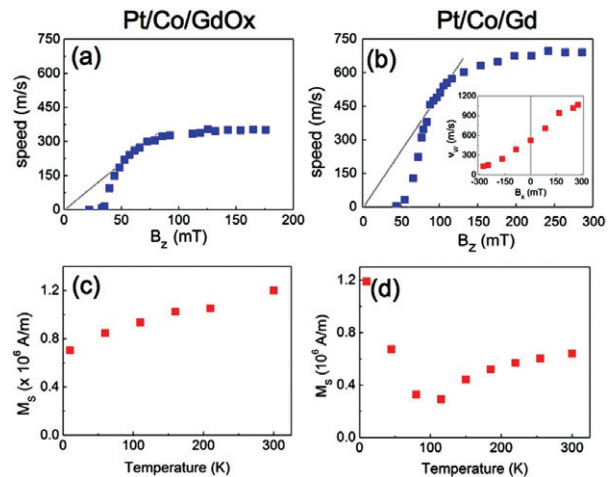

Fig. 3: (Colour online) (a), (b): DW speed *vs.* B_z field measured for Pt/Co/GdOx (a) and Pt/Co/Gd (b). Inset of (b): Walker velocity as a function of B_x. The thin lines emphasise the slope of the linear regime. (c), (d): magnetisation *vs.* temperature normalised to a $1\,\text{nm}$ thickness, measured by VSM-SQUID for Pt/Co/GdOx (c) and Pt/Co/Gd (d).

the DW structure just before the Walker breakdown [2]. In the case with disorder, the effects are qualitatively the same, as seen in fig. 2(b). As expected, the disorder induces a non-zero propagation field, but does not change the Walker field nor the maximum velocity. The shape of the DW and the energy dissipation mechanism (collapse of Bloch line pairs and creation of detached bubbles) are also not significantly affected. At fields beyond the experiment range (about $200\,\text{mT}$), the simulations reveal that the plateau ends and the DW velocity decreases. This indicates that the dissipation mechanisms can no longer sustain a constant velocity. In fact, the data show that the dissipated power reduces.

Influence of the saturation magnetisation on the maximum DW speed. – In order to address the role of the top interface on the strength of the DMI and on the maximum attainable DW velocity, we have studied samples in which the top AlOx layer was replaced by GdOx or Gd. Figures 3(a), (b) show the DW speed-*vs.*-B_z curves measured for two samples: Pt/Co/GdOx with a completely oxidised Gd layer and a Pt/Co/Gd sample where the Gd layer was not deliberately oxidised. The most striking result is that while the saturation DW speed in the Pt/Co/GdOx is of the same order of magnitude as that measured for Pt/Co/AlOx (around $300\,\text{m/s}$) the velocity in Pt/Co/Gd is a factor 2 larger.

In order to clarify this behaviour, we examined the magnetic properties of the two samples. Both samples have out-of-plane magnetic anisotropy with very similar anisotropy fields. VSM-SQUID measurements (figs. 3(c), (d)) show that the magnetisation of Pt/Co/GdOx changes weakly when going from $300\,\text{K}$ to $10\,\text{K}$: since the moment of Co is expected to change little
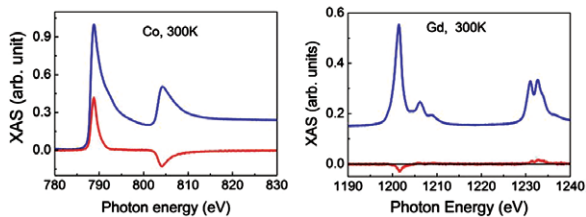
Fig. 4: (Colour online) XAS (blue line) and XMCD measurements (red line) of the Pt/Co/Gd sample at the Co $L_{2,3}$ and Gd $M_{4,5}$ edges, at 300 K and in an applied magnetic field of 1 T.

in this temperature range ($T_C \gg 300$ K), we attribute the slight decrease of the magnetisation to the presence in the sample of a small amount (less than 0.1 atomic layer) of non-oxidised Gd, which may be intermixed with the Co and acquire a moment antiparallel to that of Co. On the other hand in Pt/Co/Gd the magnetisation is strongly temperature dependent, with an increase of the magnetisation at low temperature and a minimum at around 100 K. This is the behaviour found for ferrimagnetic rare-earth/transition metal (RE-TM) compounds, where the RE moment strongly increases at low temperature while the TM moment changes little. This results in the presence of a compensation temperature, where the two sub-lattice magnetisations are equal. From this behaviour we can be confident that a large part of the Gd layer is non-oxidised in this sample, the Co and Gd layers are coupled at the interface and their moments align antiparallel to each other. Note also that while the magnetisation measured for Pt/Co/GdOx is 12.6×10^5 A/m, that of Pt/Co/Gd is 6.4×10^5 A/m at room temperature (RT). This is a clear indication that the Gd contributes to the total magnetisation even at RT.

In order to quantify the contribution of Gd to the total magnetisation in the Pt/Co/Gd sample and at RT, we carried out XMCD measurements at the Gd $M_{4,5}$ and Co $L_{2,3}$ edges. The X-ray absorption and XMCD spectra measured at 300 K in a magnetic field of 1 T are shown in fig. 4. The integrated XMCD signals can be related to the magnetic moment per absorbing atom [23,24]. A non-vanishing XMCD signal with sign opposite to that of Co is found at the Gd edge at 300 K. This emphasises: i) that part of the Gd is magnetic at RT and ii) that the Gd $4f$ and Co $3d$ moments are antiparallel. At 4 K, the Co and Gd XMCD signs are reversed and the Gd signal is much larger (not shown). This is coherent with the fact that at low temperature the Gd magnetisation increases, the total Gd moment becomes larger than that of Co and aligns with the external magnetic field.

If we suppose that the Gd intermixed with the Co at the interface has a magnetic moment similar to the one measured by López-Flores et al. [25] at 290 K (4.5 μ_B) in Gd$_{20}$Co$_{80}$, we can deduce that 10% (0.3 nm) of the Gd layer is magnetic at RT. This is the proportion of Gd atoms that is coupled to Co. In that case, we obtain that the contribution of Gd to the moment per unit surface

found by VSM-SQUID (6.4×10^{-4} A) is -4.1×10^{-4} A, while the contribution of Co is 10.5×10^{-4} A. For a Co thickness of 1 nm, this corresponds to $M_{s,Co} = 10.5 \times 10^5$ A/m, in reasonable agreement with the one obtained from XMCD ($M_s = 14 \times 10^5$ A/m) and that of Co found, e.g., in the Pt/Co/GdOx sample.

Let us now see what is the effect of the different spontaneous magnetisation of Pt/Co/GdOx and Pt/Co/Gd on the DW dynamics. Following Thiaville et al. [2] for samples with strong DMI the DW speed at the Walker field is given by

$$v_W = \gamma_0 \frac{\Delta}{\alpha} H_W \approx \frac{\pi}{2} \gamma_0 H_{DMI} \Delta = \frac{\pi}{2} \gamma_0 \frac{D}{M_s}. \qquad (1)$$

Therefore, v_W is related to the $H_{DMI}\Delta$ product, and does not depend on α. This is intuitive, as the DMI field increases the Walker field, and the widening of the DW increases the mobility. Indeed for the Pt/Co/Gd sample, where the speed is enhanced, a larger DMI field and a larger DW width are found (table 1). By inserting in eq. (1) the experimental H_{DMI} and the calculated DW width parameter, we obtain that within this model the ratio between the Walker velocities in Pt/Co/Gd and Pt/Co/GdOx is ≈ 1.90. This is very close to the ratio 1.8 between the experimental values of the DW velocities at the end of the linear regime (570 m/s for Pt/Co/Gd and 320 m/s for Pt/Co/GdOx), and even closer to the ratio of the terminal velocities (1.9).

The second part of eq. (1) shows that, very interestingly, v_W is simply proportional to D/M_s. One of the sources of the large difference in the saturation DW velocities found for Pt/Co/GdOx and Pt/Co/Gd is therefore the very different spontaneous magnetisation. In order to check whether the difference in the DW velocities may also be affected by the DMI strength, we have extracted the D values from the experimental H_{DMI} fields (table 1). Very similar D values varying between 1.5 and 1.7 mJ/m^2 are obtained for the two samples[2]. Since the Pt/Co interfaces are very similar in the two samples (they were grown in the same run) and hence contribute equally to the global DMI strength, our measurements suggest that the top Co interfaces give similar contributions to the global DMI.

We thus conclude that the large difference in the saturation DW velocities found for the asymmetric samples treated in this work is related mainly to the very different magnetisation. However, we anticipate that the maximum attainable DW velocity may be optimised by tuning the magnetisation of the magnetic layer as well as the DMI strength. Moreover, the measurement of v_W should provide a parameter-free estimation of the DMI strength. The suppression of the Walker breakdown in samples with DMI creates a speed plateau that may ease the estimation of v_W in cases in which the propagation field may be relatively

---

[2]The extracted values of D depend on the exchange stiffness A, the only material parameter that we could not measure. The best agreement with the D values measured with BLS spectroscopy is obtained using $A = 16$ pJ/m.

large, hiding the linear regime. We alert that, although the plateau velocity seems to be close to v_W with the parameters used in this work, this may not always be the case. The relation between v_W and the plateau velocity is not straightforward and deserves further study.

Conclusion. – We have shown that the DMI stabilises chiral Néel walls and allows reaching very large field-driven DW velocities. The velocity saturates beyond the Walker field and no breakdown is observed, as already found in Co/Ni/Co ultrathin films [11]. We demonstrate experimentally that, in agreement with the 1D model [2], the Walker velocity is proportional to the ratio D/M_s, so that its measurement may provide a direct method to obtain the DMI strength.

$$* * *$$

REFERENCES

[1] Parkin S., Hayashi M. and Thomas L., *Science*, **320** (2008) 190.

[2] Thiaville A., Rohart S., Jué E., Cros V. and Fert A., *EPL*, **100** (2012) 57002.

[3] Moore T. A., Miron I. M., Gaudin G., Serret G., Auffret S., Rodmacq B., Schuhl A., Pizzini S., Vogel J. and Bonfim M., *Appl. Phys. Lett.*, **93** (2008).

[4] Miron I. M., Moore T., Szambolics H., Buda-Prejbeanu L. D., Auffret S., Rodmacq B., Pizzini S., Vogel J., Bonfim M., Schuhl A. and Gaudin G., *Nat. Mater.*, **10** (2011) 419.

[5] Ryu K.-S., Thomas L., Yang S.-H. and Parkin S., *Nat. Nanotechnol.*, **8** (2013) 527.

[6] Emori S., Bauer U., Ahn S.-M., Martinez E. and Beach G., *Nat. Mater.*, **12** (2013) 611.

[7] Je S.-G., Kim D.-H., Yoo S.-C., Min B.-C., Lee K.-J. and Choe S.-B., *Phys. Rev. B*, **88** (2013) 214401.

[8] Hrabec A., Porter N. A., Wells A., Benitez M. J., Burnell G., McVitie S., McGrouther D., Moore T. A. and Marrows C. H., *Phys. Rev. B*, **90** (2014) 020402.

[9] Lavrijsen R., Hartmann D. M. F., van den Brink A., Yin Y., Barcones B., Duine R. A., Verheijen M. A., Swagten H. J. M. and Koopmans B., *Phys. Rev. B*, **91** (2015) 104414.

[10] Vaňatka M., Rojas-Sánchez J.-C., Vogel J., Bonfim M., Thiaville A. and Pizzini S., *J. Phys.: Condens. Matter*, **27** (2015) 32002.

[11] Yoshimura Y., Kim K.-J., Taniguchi T., Tono T., Ueda K., Hiramatsu R., Moriyama T., Yamada N., Nakatani Y. and Ono T., *Nat. Phys.*, **12** (2016) 157.

[12] Yamada K. and Nakatani Y., *Appl. Phys. Express*, **8** (2015) 093004.

[13] Jué E., Safeer C., Drouard M., Lopez A., Balint P., Buda-Prejbeanu L., Boulle O., Auffret S., Schuhl A., Manchon A., Miron I. and Gaudin G., *Nat. Mater.*, **15** (2016) 272.

[14] Jué E., Thiaville A., Pizzini S., Miltat J., Sampaio J., Buda-Prejbeanu L. D., Rohart S., Vogel J., Bonfim M., Boulle O., Auffret S., Miron I. M. and Gaudin G., *Phys. Rev. B*, **93** (2016) 014403.

[15] Metaxas P. J., Jamet J. P., Mougin A., Cormier M., Ferré J., Baltz V., Rodmacq B., Dieny B. and Stamps R. L., *Phys. Rev. Lett.*, **99** (2007) 217208.

[16] Dzyaloshinskii I. E., *Sov. Phys. JETP*, **5** (1957) 1259.

[17] Moriya T., *Phys. Rev.*, **120** (1960) 91.

[18] Fert A., *Mater. Sci. Forum*, **59-60** (1990) 439.

[19] Pizzini S., Vogel J., Rohart S., Buda-Prejbeanu L., Jué E., Boulle O., Miron I., Safeer C., Auffret S., Gaudin G. and Thiaville A., *Phys. Rev. Lett.*, **113** (2014) 047203.

[20] Belmeguenai M., Adam J.-P., Roussigné Y., Eimer S., Devolder T., Kim J.-V., Cherif S., Stashkevich A. and Thiaville A., *Phys. Rev. B*, **91** (2015) 180405(R).

[21] Tetienne J., Hingant T., Martìnez L., Rohart S., Thiaville A., Herrera Diez L., Garcia K., Adam J.-P., Kim J.-V., Roch J.-F., Miron I., Gaudin G., Vila L., Ocker B., Ravelosona D. and Jacques V., *Nat. Commun.*, **5** (2014) 6733.

[22] Vansteenkiste A., Leliaert J., Dvornik M., Helsen M., Garcia-Sanchez F. and Van Waeyenberge B., *AIP Adv.*, **4** (2014).

[23] Thole B. T., Carra P., Sette F. and van der Laan G., *Phys. Rev. Lett.*, **68** (1992) 1943.

[24] Carra P., Thole B. T., Altarelli M. and Wang X., *Phys. Rev. Lett.*, **70** (1993) 694.

[25] López-Flores V., Bergeard N., Halté V., Stamm C., Pontius N., Hehn M., Otero E., Beaurepaire E. and Boeglin C., *Phys. Rev. B*, **87** (2013) 214412.